Nonpolar Resistive Switching in Ag@TiO_2 Core-Shell Nanowires.

Hugh G. Manning[†, §], *Subhajit Biswas*[§, ϕ], *Justin D. Holmes* [§, ϕ], *John J. Boland* [†, §, *]

[†] School of Chemistry, Trinity College Dublin, Dublin 2, Ireland

[§]Centre for Research on Adaptive Nanostructures and Nanodevices (CRANN) & Advanced Materials and Bioengineering Research (AMBER) Research Center, Trinity College Dublin, Dublin 2, Ireland.

[ϕ] School of Chemistry, University College Cork, Cork, Ireland

Keywords: silver, titanium dioxide, core-shell, nanowire, nonpolar resistive switching

ABSTRACT: Nonpolar resistive switching, a combination of bipolar and unipolar resistive switching, is demonstrated for the first time in a single nanowire system in contact with Ag electrodes. Exploiting Ag@TiO_2 core-shell nanowires synthesized by post-growth shell formation the switching mode is controlled by adjusting the compliance. We demonstrate ON/OFF ratios of 10^5 and 10^7 obtained for bipolar and unipolar modes respectively. In the bipolar regime, retention times could be controlled up to 10^3 s and in unipolar mode > 10^6 s were recorded. We show how the unique dual mode switching behavior is enabled by the defect rich polycrystalline material structure of the TiO_2 shell and the interaction between the Ag core and the Ag electrodes. These

results provide a foundation for engineering resistive switching behaviors for memory storage and neuromorphic applications in core-shell nanowire structures.

INTRODUCTION:

The study of one-dimensional (1D) nanostructures, such as nanotubes, nanoribbons and nanowires (NWs) has generated promising new technologies, and alternatives to conventional materials due to their unique physical and chemical behaviours, which vary from their bulk and thin-film analogues.[1] Silver (Ag) based nanomaterials have attracted considerable interest with Ag nanowires (AgNWs) being employed in applications such as flexible transparent conductors, flexible thin film heaters and photovoltaics.[2-6] There is also considerable interest in the use of nanomaterials in nonvolatile memory technology, for which the switching action is controlled by the properties of both the electrodes and the dielectric materials that comprise these devices.[7] Ag for example is commonly used as an active electrode in many redox based ReRAM (resistive random access memory) cells. In cation-based ReRAM, bipolar resistive switching (BRS) devices, a low resistance state (LRS) is established through the formation of a nanoscale metallic conductive filament (CF) from an active electrode (typically Ag or Cu) through an insulator matrix. The CF is dissolved by applying a voltage of the opposite polarity, returning the cell to a high resistance state (HRS).[8] These devices have low power consumption, excellent scalability, can display ultra-fast resistive switching (RS) and have strong potential for fabricating multistate memories.[9-11] On the other hand, titanium dioxide (TiO_2) is widely used as a dielectric in ReRAM devices. As a material TiO_2 has shown promise in the areas of photocatalysis, water treatment, solar energy conversion, as well as in RS and memristive memory.[12-19]

In this paper, we describe the unique electrical properties that emerge by combining the two materials into a core (Ag) shell (TiO_2) NW structure, denoted as Ag@TiO_2 NWs. Ag@TiO_2 NWs

have already been explored for use as stable and recyclable surface enhanced Raman spectroscopy substrates, and efficient photocatalytic materials but to date the electrical behaviors of Ag@TiO_2 NWs have not been described. Typical ReRAM cells are constructed as planar metal-insulator-metal (MIM) stacks using a top-down approach, the bottom-up approach using self-assembled, and engineered nanostructures offer an alternative platform to investigate the RS phenomenon.[20] The core-shell (CS) structure allows for the ability to control and engineer the properties of the shell (such as thickness and composition) which serves as the active switching layer. The conductive core can act as both an interconnect and ion reservoir for the formation of bridging nano-filaments. The RS characteristics of CSNWs have been investigated in Ni@NiO,[21-22] Cu@CuO_x,[23] Cu@SiO_2,[7] Sn-doped In_2O_3@HfO_2,[24] Au@Ga_2O_3,[25] and at the junction of a Si@amorphous-Si NWs and crossing Ag metal lines.[26] Recently, Ag@AgO_x CSNWs were deliberately designed in a nanowire network to augment transparent electrodes with RS functionalities.[27] We report here on the unique types of RS behaviors that emerge from coating AgNWs with TiO_2. In our case, AgNWs were coated with sheaths of TiO_2 of varying crystalline qualities depending on fabrication methods, in this study both polycrystalline and amorphous TiO_2 shells were investigated with both passive and active electrode combinations. These wires can be synthesized in bulk and are stable in solution. Controlling the crystallinity of TiO_2 allows for the otherwise amorphous matrix to become more robust and provide favorable diffusion pathways for mobile Ag ions, which we show to be key to the RS process.[28]

Unipolar resistive switching (URS) involves the formation of CFs through an insulating material which are stable when the voltage bias is removed or inverted. Under larger current application, increased joule heating causes the dissolution of this connection. Due to the large currents needed to RESET the device, the power requirements for URS are much higher, and write-endurance

lifetimes much shorter when compared to BRS.[28-29] For these reasons, the development of BRS systems have been preferred over URS systems during the past number of years. Nevertheless, extensive work on various transition metal oxide (TMO) materials demonstrating either one, or both URS and BRS has been shown for thin-film devices.[18, 30-35] The presence of both URS and BRS is termed nonpolar switching.[36] CS and TMO NW devices have shown one of either BRS or URS behaviors, with arrays of multi-layered NiO/Pt NWs demonstrating nonpolar operation[37], however, to the best of our knowledge, [20, 22, 28, 38] controllable nonpolar operation in a single NW has not yet been reported.

Here, by limiting the current allowed to flow through the device during the SET operation we demonstrate controllable nonpolar RS with extremely large HRS/LRS ratios in a single two terminal CSNW device and propose a switching mechanism that explains the existence of BRS and URS behaviors.

Methods:

AgNWs were synthesized following the polyol reduction method described by Korte et al. using polyvinylpyrrolidone (PVP) and ethylene glycol as co-mediators.[39] This method produced uniform AgNWs with the length of several microns and diameters of 63 ± 10 nm; NWs were washed with acetone and water and dried under vacuum at 60 °C.

For polycrystalline CSNWs (Ag@TiO_2(P)), a thioglycolic acid (TGA) mediated process was used.[40] In particular, 5 µL of TGA was added to 2.5 mg PVP capped AgNWs in anhydrous ethanol (8 ml) under stirring. After stirring for 30 min, 20 µL of tetrabutyl titanate (TBT) was added dropwise as a TiO_2 source into the solution under inert N_2 atmosphere. The solution was stirred for another 20 min. The final mixture was transferred into a 20 mL Teflon-lined autoclave for

solvothermal treatment at 150 °C for 10 h. The resulting sample was washed three times with water and ethanol and centrifuged at 6000 rpm before being dispersed in IPA. For the synthesis of amorphous CSNWs (Ag@TiO_2(A)), a one-step solvothermal growth method reported by Du et al. was used.[12] Transmission electron microscopy (TEM) inspection of the wires showed the polycrystalline and amorphous nature of the TiO_2 coatings, with thicknesses of 14.6 ± 1.6 nm and 31 ± 7 nm for polycrystalline and amorphous shells respectively.

Single NWs were contacted by electron beam lithography (EBL) after drop-casting a NW/isopropanol dispersion on a clean Si substrate (1 µm thermal oxide) with optical lithography-defined Ti/Au contact pads (5/25 nm). EBL-deposited electrical contacts of Au-Al (30-130 nm), or Ag-Al (100-100 nm) were deposited by thermal evaporation. Devices were capped by MMA(8.5)MAA EL 9 (MicroChem) methyl methacrylate copolymer resist to protect the devices from reacting with the ambient atmosphere. Electrical measurements were carried out at room temperature using a Keithley 4200-SCS. Imaging via scanning electron microscopy (SEM) and EBL was performed on a Zeiss Supra 40. TEM imaging was performed with a JEOL 2100 operated at 200 kV. Scanning TEM (STEM) and energy dispersive x-ray (EDX) elemental analysis was carried out using a FEI Titan microscope at 300 kV.

Results:

RS devices consisted of an Ag@TiO_2(P) CSNW and two Ag electrical contacts as shown in Figure 1(a). The CS nature of the wire was confirmed by TEM inspection, Figure 1(b) shows inclusions of Ag in the microstructure of the TiO_2 shell; the inset images show elemental maps of the Ag (yellow) and Ti (red) K-edge signals using energy dispersive x-ray (EDX) analysis recorded during scanning transmission electron microscopy (STEM). Similar inclusions were found in the

amorphous TiO_2 shells of the CSNWs synthesized by the one-step solution route. These inclusions are likely the result of Ag ion migration during the solvothermal treatment at elevated temperature (~150 °C) in both synthesis methods, their presence may impact the RS properties of the CSNWs and will be discussed later. HRTEM image of the Ag@TiO_2(P) CSNW is given in Figure 1(c), the magnified region of the CS interface demonstrates the single crystalline nature of the AgNW and polycrystalline structure of the TiO_2 shell (Figure 1(d)). Fast Fourier transform (FFT) pattern from the shell region confirms the polycrystalline rutile crystal structure of the TiO_2 shell. Additional HRTEM image of Ag@TiO_2(P) and EDX mapping of the inclusions observed in the amorphous shell can be found in the supporting information (c.f Figure S1, S2).

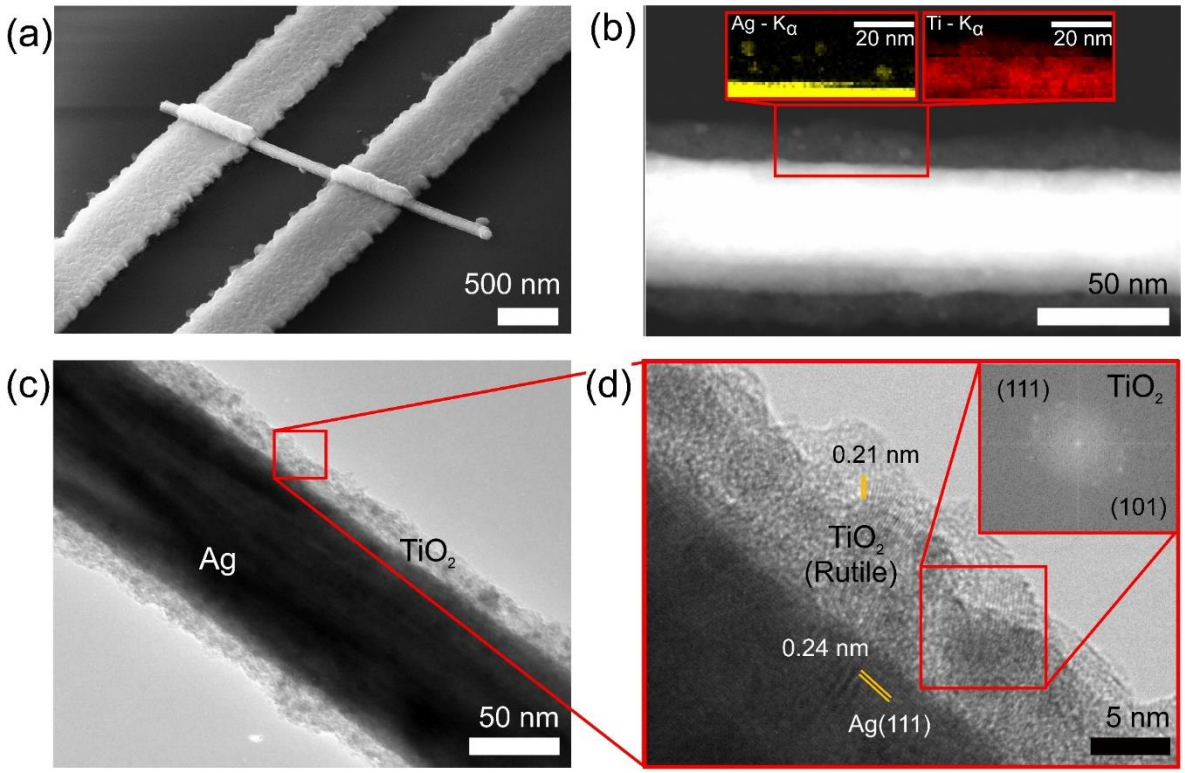

Figure 1. (a) SEM of a two-terminal Ag@TiO_2(P) device contacted with Ag electrodes. (b) STEM image of Ag@TiO_2(P) CSNW, insets showing an EDX area scan on the core/shell interface, inclusions of Ag can be found in the shell as indicated by the Ag (yellow) and Ti (red) K-alpha images. (c) HRTEM image of a Ag@TiO_2(P) CSNW. (d) Magnified area of (c) showing the single crystalline Ag core, and regions of the shell composed of rutile TiO_2, inset is a FFT pattern of the polycrystalline TiO_2 shell.

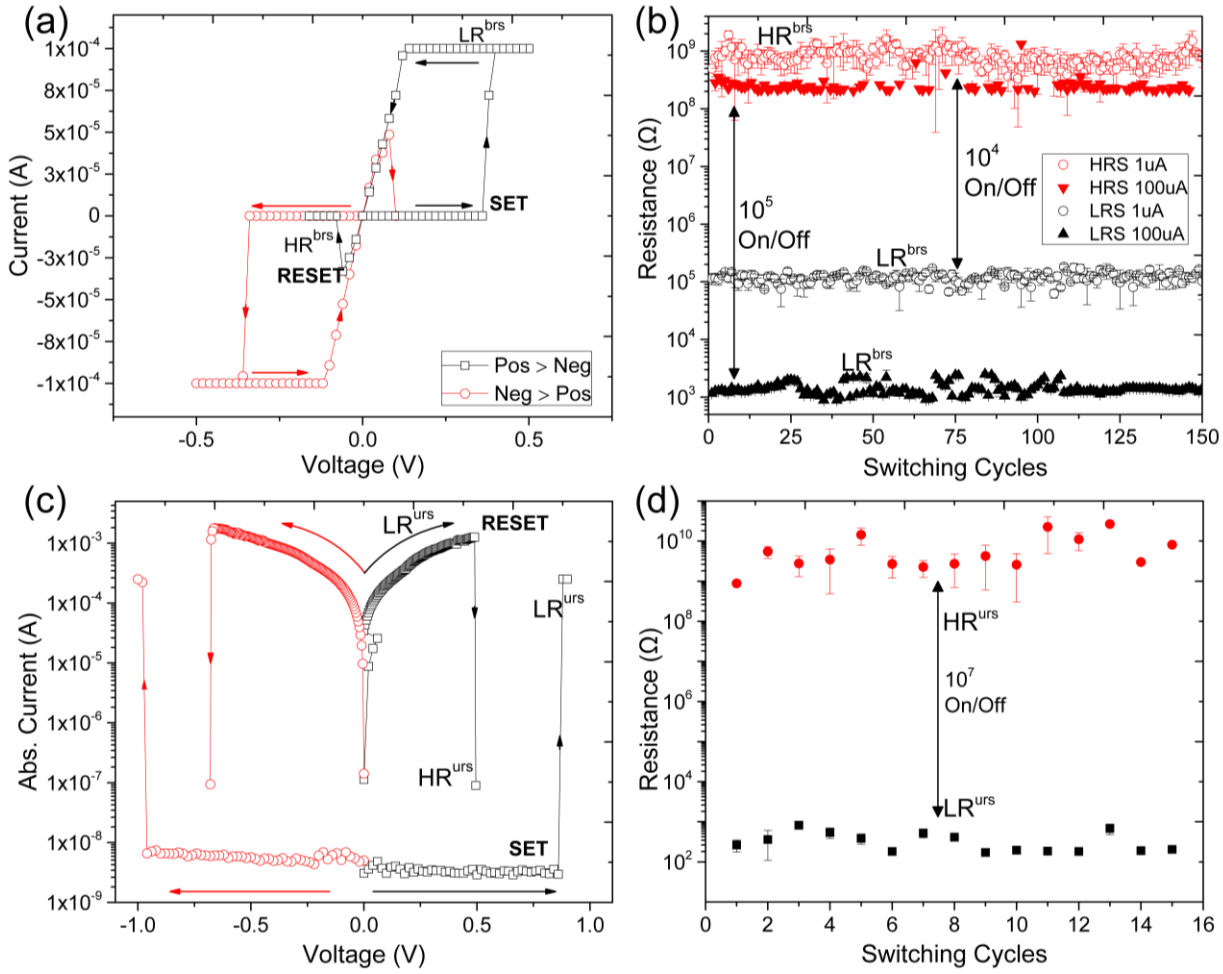

Figure 2. (a) Typical I-V characteristics of the individual Ag@TiO_2(P) CSNW device operating in the bipolar regime SET (from HRS to LRS) to a I_{CC} of 100 μA. (b) HRS and LRS by cycling the forward bias test of (a) multiple times at 1 μA (hollow circle) and 100 μA (shaded triangle) I_{CC}. (c) Typical I-V characteristic in the unipolar regime, I_{CC} for SET was 250 μA, with the I_{CC} being removed for the RESET (from LRS to HRS). (d) Repeating SET and RESET procedures of (c) in the forward bias only. LRS and HRS resistances were read at 0.5 mV.

Figure 2(a) shows typical I-V curves for Ag@TiO_2(P) NWs with Ag electrodes. CSNWs contacted with a pair of Au electrodes displayed only volatile low current switching behavior, known as threshold switching with failure of the device occurring at currents larger than 1 μA

(Figure S3 in supporting information). These findings confirm that even for CSNW systems containing electrochemically active metals (Ag core/inclusions) the choice of electrode metal is as crucial here as it is for planar thin-film devices.[17, 35, 41] As the voltage is swept in the positive direction no current is collected until the device reaches a SET state at 0.4 V, then the current jumps six orders of magnitude to the predefined compliance current (I_{CC}) and enters into a bipolar low resistance state LR^{BRS}, when the voltage is decreased towards zero the device is ohmic on the return trace with a resistance of 1-2 kΩ. As the voltage continues to be swept in the negative bias direction the current follows linearly until the device experiences a RESET event at -0.1 V and enters the bipolar high resistance state HR^{BRS} with a resistance >100 MΩ. Continuing the sweep in the negative direction causes a second SET event, this can be seen in the red curve of Figure 2(a). The BRS is repeatable over a hundred cycles and displays an ON/OFF ratio of 10^5 as seen in Figure 2(b). By controlling the value of I_{CC} it is possible to control the LR^{BRS}, though at the cost of a reduced ON/OFF ratio (Figure 2(b)). It should be noted that Ag@TiO_2(A) CSNWs contacted with two Ag electrodes failed to demonstrate BRS switching. Ag@TiO_2(A) devices experienced a SET event to a LRS state but were unable to be RESET, remaining in a LRS under the application of a negative bias, I-V curves are shown in the supporting information (c.f Figure S4). Clearly, the polycrystalline TiO_2 shell offer diffusion pathways which are necessary for the controlled switching in polycrystalline TiO_2, these are not present in the homogeneous amorphous phase TiO_2 CSNWs, this will be discussed later.

The alternative unipolar switching regime for Ag@TiO_2(P) can be accessed by programming a high SET I_{CC} (>150 μA). The URS I-V trace is shown in Figure 2(c), the voltage is increased until a SET event is reached at 0.96 V, at which point the device switches to the unipolar low resistance state LR^{URS} which is typically ~ 300 Ω. To RESET the device, the I_{CC} is removed and the device

reaches very high current levels by increasing the voltage. At a few 100 µAs to mAs the current level suddenly drops to establish the HR^{URS} (which is of a higher resistance than the HR^{BRS}); for the sweep shown in Figure 2(c) the device RESETs for 1.3 mA. Cycling the URS in Figure 2(d) shows an ON/OFF ratio of 10^7. After the device is RESET to the HR^{URS} it may be SET to the LR^{URS} in the opposite voltage direction. By reducing I_{CC} it may also be SET to the LR^{BRS}, this will be demonstrated later in the manuscript. The corresponding amorphous Ag@TiO_2(A) devices could not be RESET (see supporting information for the I-V curve and SEM image (c.f Figure S5)); when the I_{CC} was removed and a voltage sweep applied the device showed a typical RESET curve, however, it could not be subsequently SET; SEM imaging revealed that the shell had ruptured and the device had failed.

As mentioned previously, the BRS and URS can be selected by setting the I_{CC} level. To further investigate the transition between switching behaviors, I-V sweeps with increasing I_{CC} levels were applied until the device transitioned from the BRS to the URS regime. The results from this test are summarized in Figure 3(a), BRS behavior for I_{CC} levels from 50 to 125 µA is presented. At I_{CC} = 150 µA, the device remains in a LRS at negative voltages, consistent with a transition to URS behavior. It is also clear that the on-state resistance of the device is controlled by the magnitude of the I_{CC}, as seen by the change in the slopes of the return current trace from I_{CC} down to 0 voltage bias (Figure 3(a)). Through manipulation of the I_{CC}, controllable URS and BRS is demonstrated in Figure 3(b). URS was achieved with a I_{CC} = 200 µA which resulted in a LRS of 200-400 Ω (bottom right inset I-V curve). The LR^{URS} was RESET by removing the current compliance and following the top right inset I-V curve. I_{CC} = 10 µA resulted in repeatable BRS as shown in the middle-inset panel. To determine the effect of the I_{CC} level on the stability of the CF, a sequence of ten (1.7 s) SET pulses were launched into the device each reaching a

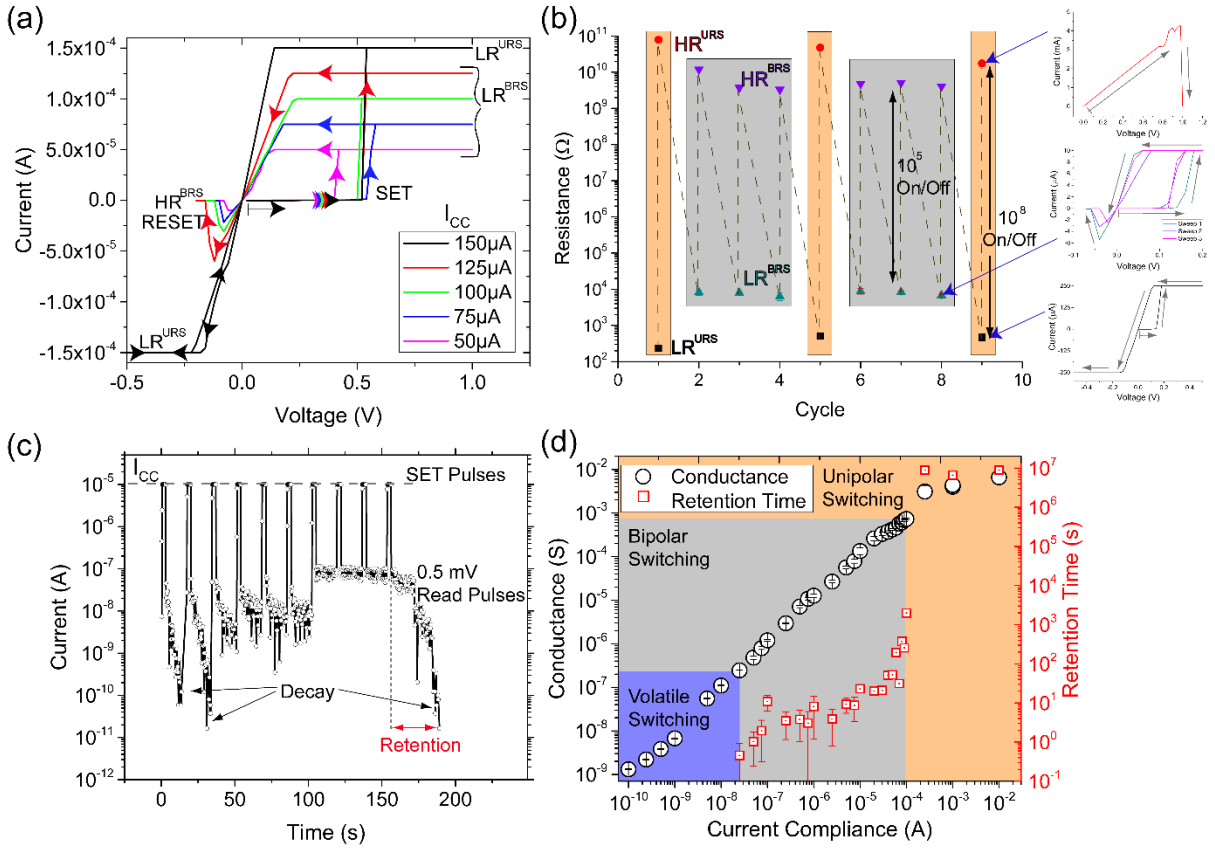

Figure 3. (a) I-V curves of increasing I_{CC} showing the transition from BRS to URS. Up to 125 μA the device RESETs at a negative bias, at 150 μA the device transitions to a URS mode. (b) Controlled operation of URS and BRS by setting a limiting I_{CC} of 200 μA and 10 μA respectively. The inset I-V curves to the right of the main panel show the URS RESET, BRS and URS behaviour (top to bottom). (c) I-t curve of ten 1.7 s pulses 15 s apart at I_{CC} = 10 μA, between each SET pulse a (150 ms) 0.5 mV pulse was applied. (d) Incrementally increasing the I_{CC} in (c) and plotting the retention time and conductance at the SET pulse against the I_{CC}. The dashed line is a linear fit to the data displaying a power law trend with exponent of 0.996. For longer retention times, the conductance of the LR^{URS} was checked each few days, then weeks at 0.5 mV.

predetermined I_{CC} (Figure 3(c)). Each SET pulse was followed by a series of 0.5 mV read pulses to interrogate the evolving resistance of the device. After the first 2 SET pulses, the device

conductance quickly drops, however following the 7th through to the 10th SET pulse the device shows a stable response which continues to be monitored by a 0.5 mV read voltage until it decays, no negative pulses were used in this test. The voltage required to reach and maintain the I_{CC} fell with each pulse, this is illustrated in Figure S6 of the supporting information.

The experiment was repeated using a range of I_{CC} SET parameters. Figure 3(d) shows the dependence of the device conductance with the I_{CC} SET values from 1 nA to 10 mA. The scaling relationship between the LRS and I_{CC} has been previously reported for thin-film programmable metallization cell (PMC) memory.[11, 32, 42-43] The same power law relationship is seen to hold for unipolar, bipolar and threshold switching. The blue shaded box in Figure 3(d) highlights the volatile threshold switching regime that occurs at low I_{CC} where the device does not retain the LRS after the voltage is removed and subsequently read, the corresponding memory retention time is zero. At higher I_{CC} the device enters the BRS regime (grey shaded box), where the conductance of the device and the retention time can be set by programming the I_{CC}. The LRS^{BRS} decays over time as previously described, and the rate of decay is controlled by the SET I_{CC}, enabling retention times of seconds, minutes and hours. When the I_{CC} is increased further the device enter the URS regime (orange shaded box), where the conductance level and retention time start to saturate. A number of devices could be SET to I_{CC} of over 1 mA, the retention time of all URS devices were stable for over 10^6 s. Histogram of SET voltages for Ag@TiO_2- (P) and (A) can be found in the supporting information (c.f Figure S7).

Many factors were considered in this study to elucidate the RS mechanism, a diagram which illustrates the relationships between the structures, I_{CC}, electrode composition and I-V performances can be found in Figure S8. The mechanistic role and observation of oxygen vacancies in the RS behaviours of TiO_2 devices has been well documented.[44] Recently dual-

filament switching behaviours have been directly observed in Ta_2O_5-based memristors.[45] However, due to the lack of controllable RS for Au contacted amorphous and polycrystalline CSNWs we do not consider oxygen vacancy species to be a determining factor in the RS mechanism though their presence is expected (further discussion and schematic is provided in the supporting information Figure S9). Based on the experimental evidence provided of RS in CSNWs contacted with Ag electrodes only, it is most likely that the switching mechanism is dominated by the formation of metallic Ag CFs facilitated by the Ag inclusions and the Ag contacts. A schematic of the SET and RESET behaviors is provided in Figure 4. We propose that under the application of a voltage bias, nanoionic redox processes occur.[28, 32, 11, 41] Ag^+ ions are formed via oxidation at the Ag anode and then migrate through the polycrystalline TiO_2 shell before being reduced at the Ag cathode. The tip of the electrodeposited filament moves back towards the anode as new Ag^+ ions arrive through the lower activation energy pathways found at the grain boundaries of polycrystalline TiO_2.[32, 46] The growth of this filament is likely to occur in a "winner takes all" scenario, with the favored CF extending out from the cathode and bridging across the entire dielectric shell.[28] The Ag inclusions in the shell are expected to lower the SET voltages by suppling an additional source of cations for the CF. Once a CF bridges the Ag electrode and the Ag core of the wire, the second junction becomes polarized and the CF growth process occurs, this can be seen in Figure 4(a). The voltages depicted in the schematic only relate to the second CF growth, the transition voltages corresponding to the two-building processes are not shown. Once both junctions are bridged by a CF current flows to reach the I_{CC} and a LRS is established. The formation of the first and then second junction sets an asymmetry in the system which at low I_{CC} allows for the bipolar behaviour. A key factor for nonpolar operation is setting the device

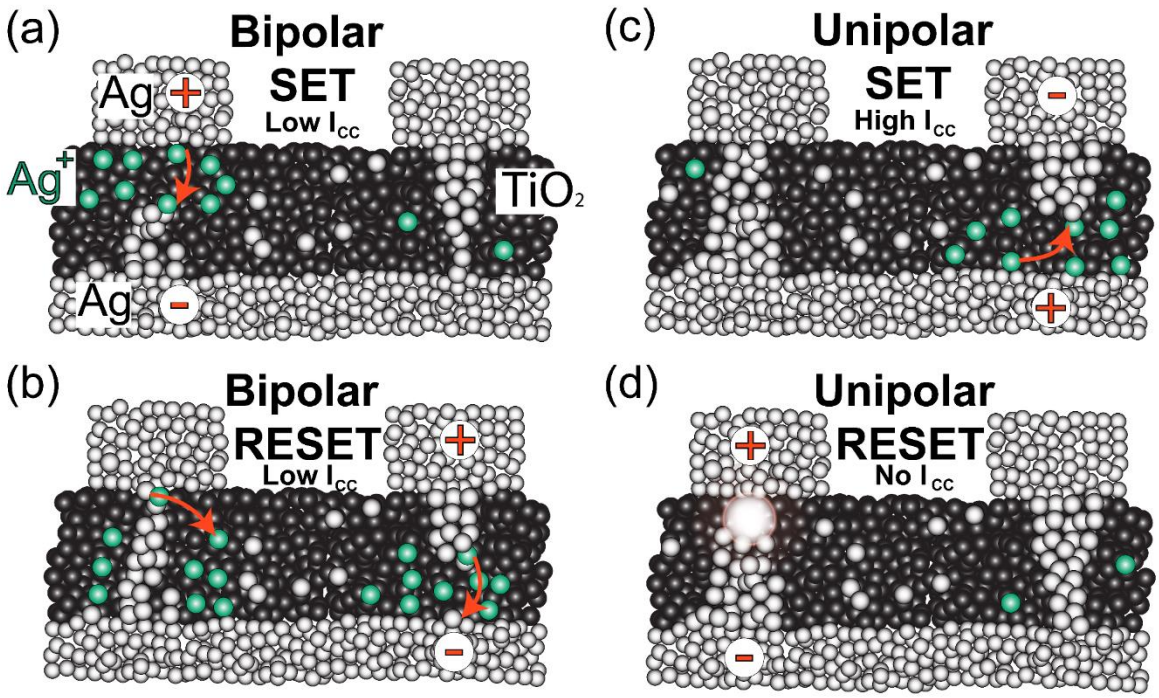

Figure 4. Schematic of SET and RESET conditions in Ag@TiO_2(P) CSNWs. (a) Under low I_{CC} conditions, bipolar SET is caused by the growth of Ag metallic filaments from the cathode toward the anode due to oxidation and subsequent electrodeposition of Ag to Ag^+ ions (shown as the movement of green spheres via red arrows). (b) Under bias inversion the conductive filament is withdrawn due to the same process and breaks. (c) With a higher I_{CC} imposed, a stronger filament can form, which is thicker and more robust than that formed in (a). (d) RESET of the URS due to thermal breakdown (depicted as a radial hot spot) of the CF caused by Joule heating under high current flow with on I_{CC}.

resistance and limiting CF growth by setting the I_{CC}. At very low I_{CC}, an incomplete CF forms which serves to reduce the tunneling gap but makes no stable bridging filament causing the threshold switching behaviour. Increasing the I_{CC} to low levels causes formation of a bridging CF which is not pronounced enough to be stable to reoxidation and can be dissolved by applying a voltage of the opposite polarity, returning the device to a HRS state (Figure 4(b)). Application of an increasing negative voltage causes the filaments to regrow, but in the opposite direction as

before (not shown schematically) due to the symmetric construction of the device. When voltage is applied with a high I_{CC}, the CF which physically bridges the Ag electrode and core can supply electrons for subsequent ion reduction allowing the CF to grow radially according to previously developed models.[10] This is expected to result in a conical shape to the CF which is wider at the base and narrows along its length,[28] as depicted in Figure 4(c). It has been previously shown for other Ag CF systems ($Ag/Ge_xS_y/W$ thin-film cells) that the retention time of the ON-state improves as the value of LRS decreases.[47] A feature which is evident from the retention times presented here. The explanation given by several authors align with the proposed mechanism given in this work, that it results from formation of a thicker, or perhaps growth of multiple metallic filaments which would be slower to erode away.[48]

The URS CF formed at high I_{CC} requires an increased contribution from Joule heating/thermal diffusion to break the connection as illustrated by the thermally dominated hotspot in Figure 4(d). The effect of Joule heating will be greatest at the narrowest part of the bridging CF, which is expected to be at the interface to the cathode.[28] Experimental evidence presented in this paper shows that polycrystalline TiO_2 CSNWs undergo controllable nonpolar RS sustaining the large currents required for the URS RESET process. Grain boundaries in polycrystalline layers are known to provide favorable diffusion pathways and enhanced charge transport for migrating species[32, 46, 48-49] which are absent in amorphous layers. This is expected to result in the formation of well-defined, discrete CFs. The same cannot be said for amorphous TiO_2 shelled NWs, where the shell is more homogeneous and the nanowires ruptured when subjected to large current densities. (See the supporting information for the I-V curve and SEM image (Figure S5)).

It is interesting to contrast our results with those reported in the literature, Ag/TiO_2 combinations have been explored in conventional thin-film two-terminal memory cells, examples of these can

be found in TABLE 1. In the work by Hu et al. URS switching was reported with 200 μm^2 Ag contacts and an amorphous 50 nm TiO_2 dielectric spacer. SET voltages of 1 V were observed, with large SET and RESET currents of 10 mA and 20 mA respectively reported.[35] Using a 100 μm diameter Ag top electrode and an inert Pt bottom electrode, Tsunoda et al. demonstrated BRS in 40 nm polycrystalline/rutile TiO_2 films, with SET voltages of 0.23 V.[32] Similar voltages are required for the RS in this study, the large diameter Ag top electrode and antisymmetric nature of the device is expected to result in bipolar operation. Finally, Ghenzi et al. reports a device with a polycrystalline anatase TiO_2 layer with millimeter sized contacts showing initial URS behavior which lasts for a hundred cycles then transforms into a BRS only device. While this system demonstrates nonpolar operation, switching between these BRS and URS was not shown to be controllable.[17]

The nonpolar switching observed in our study has some important advantages over the previously reported thin-film devices in TABLE 1. It is the only system to show controllable nonpolar operation. It is the first report observing nonpolar operation in a CSNW structure, the SET and RESET currents observed in CSNWs are significantly lower than those detailed for the relatively large thin film devices. This is attributed to the reduced contact area over which the applied electric field acts, which in turn leads to a focused CF growth with a reduced number of competing leakage channels. Scaling effects were shown to have a consequence on the unipolar and bipolar behaviors of thin-film devices, as shown by the work of Yanagida et al.[30] CSNWs also require the formation of two junctions, the asymmetry set in the device by forming one connection and then the other could facilitate the BRS behaviours at low I_{CC} values and URS responses at high I_{CC}.

TABLE 1. Two Terminal Thin Film Memory Cells That Have Been Previously Reported, RS Types and ON/OFF Ratios.

author	memory cell	switching type	ON/OFF ratio
Hu et al.[35]	Ag/50 nm TiO_2/Ag	URS	10^2
Tsunoda et al.[32]	Ag/40 nm TiO_2/Pt	BRS	10^8
Ghenzi et al.[17]	Ag/100 nm TiO_2/Si	BRS & URS	10 (BRS) 10^4(URS)
This work.	Ag/30 nm TiO_2/Ag	BRS & URS	10^5(BRS) 10^7(URS)

Conclusions:

In summary, we have investigated the requirements for RS in Ag@TiO_2 CSNW devices. CSNWs were synthesized by two methods resulting in either amorphous or polycrystalline rutile TiO_2 shells surrounding an Ag core. HRTEM and EDX analysis identified the presence of Ag inclusions in the shell of both batches of CSNWs. Neither nanowire system showed controllable RS when contacted with Au electrodes, while dual mode operation of BRS and URS, known as nonpolar RS was observed in CSNWs with polycrystalline TiO_2 coatings contacted with Ag electrodes. The absence of RS in Au contacted Ag@TiO_2(P) demonstrates that the interplay between the Ag electrodes, Ag inclusions and the Ag core is key to device operation. Operation of BRS and URS could be selected by defining the I_{CC}, resistance levels differed between URS and BRS modes, allowing them to be readily distinguished, and we postulate the Ag CF associated with the two switching modes are directly related. BRS was demonstrated with over 150 cycles and a tunable retention time up to 10^3 seconds; the conductance of the SET state could also be controlled by programming the pre-defined I_{CC}. ON/OFF ratios were dependent on the I_{CC} as were memory retention times, ON/OFF ratios and memory retention were found to be highest in URS

modes of 10^7 and $>10^6$ s respectively. These findings are important in the development of CSNW systems and highlight the influence of the shell microstructure material and electrode composition. Moreover, the CSNW system is complimentary to thin film studies, displaying how RS behaviors can be unpredictable as devices are scaled to nm dimensions. Furthermore, it is the first report of controllable nonpolar operation in a single nanowire system; nonpolar operation allows for functional flexibility between short term and long term memory which is important for hardware based neuromorphic applications. Future work will include assembly of these CSNWs into randomly orientated nanowire networks and considering other core and shell material combinations to engineer resistive and memristive behaviors.

Supporting Information.

Further information on the amorphous shelled CSNWs, including TEM and STEM analysis, identifying Ag inclusions in the TiO_2 shell. Electrical data such as threshold switching of these wires with Au electrodes, and URS SET with Ag electrodes. Electrical data of attempted URS RESET and subsequent SEM imaging. A diagram considering all experimental variables, and a schematic and discussion related to Au contacted Ag@TiO_2 are also included (PDF).

Corresponding Author

*E-mail: jboland@tcd.ie

Author Contributions.

H.G.M wrote the paper and performed all experiments. S.B synthesized both batches of CS Ag-TiO_2 NWs. J.T.H and J.J.B led overall effort and co-wrote the paper. All authors discussed and commented on the manuscript and on the results.

Conflict of Interest: The authors declare no competing financial interest.

Acknowledgements.

The authors wish to acknowledge funding from the European Research Council under Advanced Grant 321160. This publication has emanated from research supported in part by a research grant from Science Foundation Ireland (SFI) AMBER Centre under Grant Number SFI/12/RC/2278. The facilities and staff at the Advanced Microscopy Laboratory at Trinity College Dublin are acknowledged for their support, in particular, the TEM work performed by Dr. Eoin McCarthy.

REFERENCES

1. Hu, J.; Odom, T. W.; Lieber, C. M., Chemistry and physics in one dimension: synthesis and properties of nanowires and nanotubes. *Accounts of chemical research* **1999,** *32* (5), 435-445.
2. Langley, D.; Giusti, G.; Mayousse, C.; Celle, C.; Bellet, D.; Simonato, J.-P., Flexible transparent conductive materials based on silver nanowire networks: a review. *Nanotechnology* **2013,** *24* (45), 452001.
3. Li, B.; Ye, S. R.; Stewart, I. E.; Alvarez, S.; Wiley, B. J., Synthesis and Purification of Silver Nanowires To Make Conducting Films with a Transmittance of 99%. *Nano Letters* **2015,** *15* (10), 6722-6726.
4. Gomes da Rocha, C.; Manning, H. G.; O'Callaghan, C.; Ritter, C.; Bellew, A. T.; Boland, J. J.; Ferreira, M., Ultimate Conductivity Performance in Metallic Nanowire Networks. *Nanoscale* **2015,** *7* (30), 13011-13016.
5. Bellew, A. T.; Manning, H. G.; Gomes da Rocha, C.; Ferreira, M. S.; Boland, J. J., Resistance of Single Ag Nanowire Junctions and Their Role in the Conductivity of Nanowire Networks. *ACS nano* **2015,** *9* (11), 11422-9.
6. O'Callaghan, C.; Gomes da Rocha, C.; Manning, H.; Boland, J. J.; Ferreira, M., Effective medium theory for the conductivity of disordered metallic nanowire networks. *Physical Chemistry Chemical Physics* **2016,** *18* (39), 27564-27571.

7. Catenacci, M. J.; Flowers, P. F.; Cao, C. Y.; Andrews, J. B.; Franklin, A. D.; Wiley, B. J., Fully Printed Memristors from Cu-SiO2 Core-Shell Nanowire Composites. *Journal of Electronic Materials* **2017,** *46* (7), 4596-4603.
8. Valov, I., Redox-Based Resistive Switching Memories (ReRAMs): Electrochemical Systems at the Atomic Scale. *ChemElectroChem* **2014,** *1* (1), 26-36.
9. Jameson, J.; Blanchard, P.; Cheng, C.; Dinh, J.; Gallo, A.; Gopalakrishnan, V.; Gopalan, C.; Guichet, B.; Hsu, S.; Kamalanathan, D. In *Conductive-bridge memory (CBRAM) with excellent high-temperature retention*, Electron Devices Meeting (IEDM), 2013 IEEE International, IEEE: 2013; pp 30.1. 1-30.1. 4.
10. Russo, U.; Kamalanathan, D.; Ielmini, D.; Lacaita, A. L.; Kozicki, M. N., Study of multilevel programming in programmable metallization cell (PMC) memory. *Electron Devices, IEEE Transactions on* **2009,** *56* (5), 1040-1047.
11. Valov, I.; Kozicki, M. N., Cation-based resistance change memory. *Journal of Physics D: Applied Physics* **2013,** *46* (7), 074005.
12. Du, J.; Zhang, J.; Liu, Z.; Han, B.; Jiang, T.; Huang, Y., Controlled synthesis of Ag/TiO2 core-shell nanowires with smooth and bristled surfaces via a one-step solution route. *Langmuir* **2006,** *22* (3), 1307-1312.
13. Lee, S.-Y.; Park, S.-J., TiO 2 photocatalyst for water treatment applications. *Journal of Industrial and Engineering Chemistry* **2013,** *19* (6), 1761-1769.
14. Wang, G.; Wang, H.; Ling, Y.; Tang, Y.; Yang, X.; Fitzmorris, R. C.; Wang, C.; Zhang, J. Z.; Li, Y., Hydrogen-treated TiO2 nanowire arrays for photoelectrochemical water splitting. *Nano letters* **2011,** *11* (7), 3026-3033.
15. Strukov, D. B.; Snider, G. S.; Stewart, D. R.; Williams, R. S., The missing memristor found. *nature* **2008,** *453* (7191), 80-83.
16. O'Kelly, C.; Fairfield, J. A.; Boland, J. J., A Single Nanoscale Junction with Programmable Multilevel Memory. *ACS Nano* **2014,** *8* (11), 11724-9.
17. Ghenzi, N.; Stoliar, P.; Fuertes, M. C.; Marlasca, F. G.; Levy, P., Resistive switching in Ag–TiO2 contacts. *Physica B: Condensed Matter* **2012,** *407* (16), 3096-3098.
18. Kwon, D.-H.; Kim, K. M.; Jang, J. H.; Jeon, J. M.; Lee, M. H.; Kim, G. H.; Li, X.-S.; Park, G.-S.; Lee, B.; Han, S., Atomic structure of conducting nanofilaments in TiO2 resistive switching memory. *Nature nanotechnology* **2010,** *5* (2), 148-153.
19. O'Kelly, C. J.; Fairfield, J. A.; McCloskey, D.; Manning, H. G.; Donegan, J. F.; Boland, J. J., Associative Enhancement of Time Correlated Response to Heterogeneous Stimuli in a Neuromorphic Nanowire Device. *Advanced Electronic Materials* **2016,** *2* (6).
20. Ielmini, D.; Cagli, C.; Nardi, F.; Zhang, Y., Nanowire-based resistive switching memories: devices, operation and scaling. *Journal of Physics D: Applied Physics* **2013,** *46* (7), 074006.
21. Cagli, C.; Nardi, F.; Harteneck, B.; Tan, Z.; Zhang, Y.; Ielmini, D., Resistive-Switching Crossbar Memory Based on Ni–NiO Core–Shell Nanowires. *Small* **2011,** *7* (20), 2899-2905.
22. He, L.; Liao, Z. M.; Wu, H. C.; Tian, X. X.; Xu, D. S.; Cross, G. L. W.; Duesberg, G. S.; Shvets, I. V.; Yu, D. P., Memory and Threshold Resistance Switching in Ni/NiO Core-Shell Nanowires. *Nano Letters* **2011,** *11* (11), 4601-4606.
23. Liang, K.-D.; Huang, C.-H.; Lai, C.-C.; Huang, J.-S.; Tsai, H.-W.; Wang, Y.-C.; Shih, Y.-C.; Chang, M.-T.; Lo, S.-C.; Chueh, Y.-L., Single CuO x nanowire memristor: forming-free resistive switching behavior. *ACS applied materials & interfaces* **2014,** *6* (19), 16537-16544.

24. Huang, C.-H.; Chang, W.-C.; Huang, J.-S.; Lin, S.-M.; Chueh, Y.-L., Resistive switching of Sn-doped In 2 O 3/HfO 2 core–shell nanowire: geometry architecture engineering for nonvolatile memory. *Nanoscale* **2017**.
25. Hsu, C.-W.; Chou, L.-J., Bipolar resistive switching of single gold-in-Ga2O3 nanowire. *Nano letters* **2012,** *12* (8), 4247-4253.
26. Dong, Y.; Yu, G.; McAlpine, M. C.; Lu, W.; Lieber, C. M., Si/a-Si core/shell nanowires as nonvolatile crossbar switches. *Nano Letters* **2008,** *8* (2), 386-391.
27. Du, H.; Wan, T.; Qu, B.; Cao, F.; Lin, Q.; Chen, N.; Lin, X.; Chu, D., Engineering Silver Nanowire Networks: from Transparent Electrodes to Resistive Switching Devices. *ACS Applied Materials & Interfaces* **2017,** *9* (24), 20762-20770.
28. Ielmini, D.; Waser, R., *Resistive Switching: From Fundamentals of Nanoionic Redox Processes to Memristive Device Applications*. John Wiley & Sons: 2015.
29. Waser, R.; Aono, M., Nanoionics-based resistive switching memories. *Nature materials* **2007,** *6* (11), 833-840.
30. Yanagida, T.; Nagashima, K.; Oka, K.; Kanai, M.; Klamchuen, A.; Park, B. H.; Kawai, T., Scaling effect on unipolar and bipolar resistive switching of metal oxides. *Scientific reports* **2013,** *3*, 1657.
31. Zhu, Y.; Li, M.; Zhou, H.; Hu, Z.; Liu, X.; Fang, X.; Sebo, B.; Fang, G.; Zhao, X., Nonvolatile bipolar resistive switching in an Ag/TiO2/Nb: SrTiO3/In device. *Journal of Physics D: Applied Physics* **2012,** *45* (37), 375303.
32. Tsunoda, K.; Fukuzumi, Y.; Jameson, J.; Wang, Z.; Griffin, P.; Nishi, Y., Bipolar resistive switching in polycrystalline Ti O 2 films. *Applied physics letters* **2007,** *90* (11), 113501.
33. Jeong, D. S.; Schroeder, H.; Waser, R., Coexistence of bipolar and unipolar resistive switching behaviors in a Pt⁄ TiO2⁄ Pt stack. *Electrochemical and solid-state letters* **2007,** *10* (8), G51-G53.
34. Kim, K. M.; Kim, G. H.; Song, S. J.; Seok, J. Y.; Lee, M. H.; Yoon, J. H.; Hwang, C. S., Electrically configurable electroforming and bipolar resistive switching in Pt/TiO2/Pt structures. *Nanotechnology* **2010,** *21* (30), 305203.
35. Hu, Y.; Perello, D.; Yun, M.; Kwon, D.-H.; Kim, M., Variation of switching mechanism in TiO 2 thin film resistive random access memory with Ag and graphene electrodes. *Microelectronic Engineering* **2013,** *104*, 42-47.
36. Akinaga, H.; Shima, H.; Takano, F.; Inoue, I.; Takagi, H., Resistive switching effect in metal/insulator/metal heterostructures and its application for non-volatile memory. *IEEJ Transactions on Electrical and Electronic Engineering* **2007,** *2* (4), 453-457.
37. Huang, Y.-C.; Chen, P.-Y.; Chin, T.-S.; Liu, R.-S.; Huang, C.-Y.; Lai, C.-H., Improvement of resistive switching in NiO-based nanowires by inserting Pt layers. *Applied Physics Letters* **2012,** *101* (15), 153106.
38. Oliver, S. M.; Fairfield, J. A.; Bellew, A. T.; Lee, S.; Champlain, J. G.; Ruppalt, L. B.; Boland, J. J.; Vora, P. M., Quantum point contacts and resistive switching in Ni/NiO nanowire junctions. *Applied Physics Letters* **2016,** *109* (20), 203101.
39. Korte, K. E.; Skrabalak, S. E.; Xia, Y., Rapid synthesis of silver nanowires through a CuCl-or CuCl 2-mediated polyol process. *Journal of Materials Chemistry* **2008,** *18* (4), 437-441.
40. Gale, E., TiO2-based memristors and ReRAM: materials, mechanisms and models (a review). *Semiconductor Science and Technology* **2014,** *29* (10), 104004.

41. Waser, R.; Dittmann, R.; Staikov, G.; Szot, K., Redox-based resistive switching memories–nanoionic mechanisms, prospects, and challenges. *Advanced materials* **2009,** *21* (25-26), 2632-2663.
42. Mahalanabis, D.; Barnaby, H.; Gonzalez-Velo, Y.; Kozicki, M.; Vrudhula, S.; Dandamudi, P., Incremental resistance programming of programmable metallization cells for use as electronic synapses. *Solid-State Electronics* **2014,** *100*, 39-44.
43. Tappertzhofen, S.; Valov, I.; Waser, R., Quantum conductance and switching kinetics of AgI-based microcrossbar cells. *Nanotechnology* **2012,** *23* (14), 145703.
44. Jang, M. H.; Agarwal, R.; Nukala, P.; Choi, D.; Johnson, A. C.; Chen, I.-W.; Agarwal, R., Observing Oxygen Vacancy Driven Electroforming in Pt–TiO2–Pt Device via Strong Metal Support Interaction. *Nano letters* **2016,** *16* (4), 2139-2144.
45. Chang, C. F.; Chen, J. Y.; Huang, C. W.; Chiu, C. H.; Lin, T. Y.; Yeh, P. H.; Wu, W. W., Direct Observation of Dual-Filament Switching Behaviors in Ta2O5-Based Memristors. *Small* **2017,** *13* (15).
46. Mitchell, B. S., *An introduction to materials engineering and science for chemical and materials engineers*. John Wiley & Sons: 2004.
47. Kamalanathan, D.; Russo, U.; Ielmini, D.; Kozicki, M. N., Voltage-driven on–off transition and tradeoff with program and erase current in programmable metallization cell (PMC) memory. *IEEE Electron Device Letters* **2009,** *30* (5), 553-555.
48. Valov, I.; Waser, R.; Jameson, J. R.; Kozicki, M. N., Electrochemical metallization memories—fundamentals, applications, prospects. *Nanotechnology* **2011,** *22* (25), 254003.
49. Lee, M.-J.; Han, S.; Jeon, S. H.; Park, B. H.; Kang, B. S.; Ahn, S.-E.; Kim, K. H.; Lee, C. B.; Kim, C. J.; Yoo, I.-K., Electrical manipulation of nanofilaments in transition-metal oxides for resistance-based memory. *Nano letters* **2009,** *9* (4), 1476-1481.